3D-PRINTED OSTEOCHONDRAL GRAFTS AND THEIR CHARACTERIZATION

Victoria Effiong Effanga

Submitted in fulfillment of the requirements for the degree of Master of Science in Biomedical Engineering

School of Engineering and Digital Sciences
Department of Chemical and Materials Engineering
Nazarbayev University

53 Kabanbay Batyr Avenue,
Astana, Kazakhstan, 010000

Supervisor: Cevat Erisken, Ph.D.
Co-Supervisor: Dana Akilbekova, Ph.D.
Department of Chemical and Materials Engineering

April 2024

DECLARATION

I hereby declare that this manuscript, entitled “3d-Printed Osteochondral Grafts and Their Characterization”, is the result of my work except for quotations and citations which have been duly acknowledged. I also declare that, to the best of my knowledge and belief, it has not been previously or concurrently submitted, in whole or in part, for any other degree or diploma at Nazarbayev University or any other national or international institution.

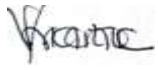

Name: Victoria Effiong Effanga

Date: 18.04.2024

Acknowledgments

I express my gratitude to God for enabling the successful completion of this work. I extend heartfelt appreciation to my supervisor Dr. Cevat Erisken, whose inspiration led us to undertake this research, and co-supervisor Dana Akilbekova, whose guidance and assistance were invaluable during this study. Additionally, I acknowledge the support provided by colleagues Fariza Mukasheva, Muhamad Moazzam, Xiao Zhao, Aida Zhakypbekova, whose contributions impacted this research. Finally, I thank my family for their unwavering support.

Table of Contents

List of abbreviations

β-GP – β-glycerophosphate disodium salt hydrate

ECM – Extracellular matrix

EDX - Energy dispersive X-Ray

FTIR - Fourier transform infrared.

Gel – Gelatine.

HAP – Hydroxyapatite

Micro-CT - Microcomputed tomography

OA – Osteoarthritis

OC Tissue– Osteochondral tissue

OXA – Oxidized alginate

PCL – Polycaprolactone

PBS – Phosphate buffer salt

SEM – scanning electron microscope

TE – Tissue engineering

TGA - Thermogravimetric analysis

List of figures

Abstract

The osteochondral (OC) interface is a complex tissue with a hierarchical structure found at the ends of the bones of the knee joint consisting of a layer of soft tissue (cartilage) overlaying hard tissue in the subchondral bone. It exhibits a gradient of its constituents, especially in terms of mineral concentration, cell phenotype, collagens, and glycosaminoglycans, with a thickness of around 0.5 mm. The tidemark, a critical yet often overlooked component of OC interface tissue, plays a pivotal role in maintaining tissue function by acting as a barrier against vascular invasion of the cartilage. Fabricating scaffolds that mimic the complex physiology and functionalities of the OC tissue within the physiological thickness remains a challenge.

This study aimed at fabricating a unitary composite scaffold that is similar of the OC interface in terms of distribution of its mineral content. It was hypothesized that the interface formed between the layers of the multilayer graft will possess a thickness of hydroxyapatite (HAP) gradient similar to that seen at the native rabbit OC tissue.

To test the hypothesis, a multilayer composite OC graft was fabricated using gelatin and oxidized alginate (OXA) compositions with and without HAP for the bone and cartilage regions, respectively, and a gradient of HAP was formed in between. The two layers were formed using a 3D bioprinting method, while a porous electrospun mesh of polycaprolactone was placed in the graded region between cartilage and bone to represent the tidemark. The change in mineral content across the rabbit OC interface tissue and the OC graft interface was investigated using energy dispersive X-ray (EDX) and micro computed tomography (μCT) characterization. The printability of the bioinks was verified by a strain sweep test, and volumetric expansion of both inks, with and without HAP, was examined using a swelling test.

Findings revealed that both bioinks exhibited a shear thinning behavior. In additssion, swelling test showed that both inks possessed similar volumetric expansion when immersed in water, demonstrating its feasibility to be used as a defect filler. EDX scan for calcium (Ca) and phosphorus (P) verified the gradient of mineral in both OC grafts and native rabbit OC tissue. The μCT characterization verified a HAP gradient created in the OC graft within 168μm thickness similar to the mineral gradient thickness determined for rabbit OC interface. Furthermore, the electrospun membrane was found to have pore diameters less than 1μm that is sufficient to prevent vascular invasion of the articular cartilage tissue.

Overall, the OC graft fabricated using combined bioprinting and electrospinning techniques demonstrated a potential to serve as a biomimetic hydrogel filler for regenerating OC defects to restore the function of the knee joint. It is expected that the proposed OC graft will be effectively used to address a significant clinical problem that affects millions of people, with significant societal and economic impacts.

Chapter 1 - Introduction

1.1 The Osteochondral Tissue

The OC tissue is a complex tissue with a hierarchical structure found at the ends of the synovial joint bones. It is primarily divided into two main regions, the articular cartilage and the subchondral bone, with a thin interface between the two (as depicted in Figure 1). These regions consist of distinct cell types and collagen arrangements. Specifically, the cartilage region encompasses the superficial zone, middle zone, deep zone, and calcified cartilage, while the bone region includes the cement line and subchondral bone. The tidemark serves as the boundary separating these two distinct yet continuous regions.

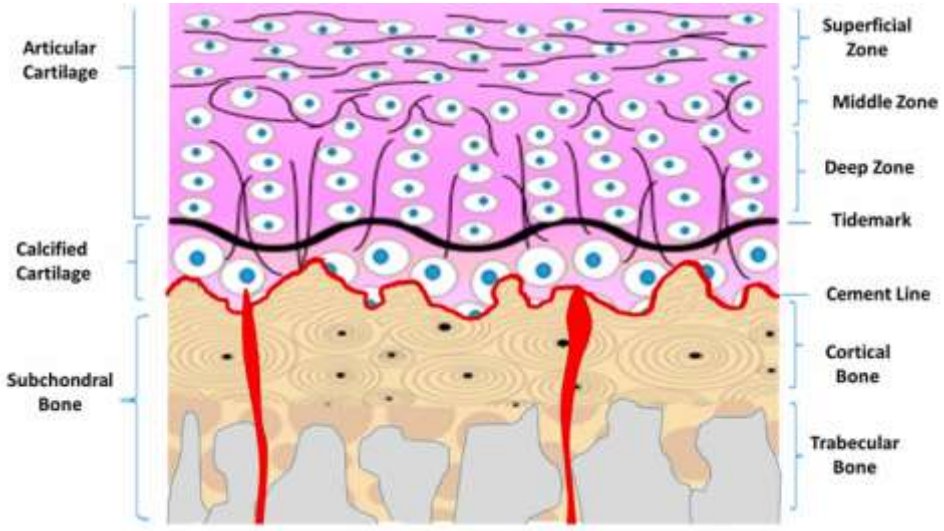

Figure 1: Schematic representation of the osteochondral tissue and its hierarchical structure [1]

The articular cartilage is an avascular and hypocellular tissue primarily consisting of chondrocytes, which makes up about 3 -5% of the tissue, and the extracellular matrix (ECM) (collagen, water, non-collagenous protein, and proteoglycans) makes up the rest of the tissue[1][2].This tissue exhibits a sponge-like behavior, expelling and absorbing water under compression and relaxation, respectively [2]. The superficial zone is the topmost layer of the cartilage. It consists of tightly packed collagen arranged parallel to the surface. Because of the synovial fluid present in the joint, this layer helps to maintain lubrication [3]. The Middle zone, which is located below the superficial zone contains chondrocytes with an oblique orientation with sparce distribution. Proteoglycans are the most abundant ECM component in this region. Proteoglycans play a crucial role in absorbing shock and resisting compressive stress without

harming the subchondral bone [3]. The next zone found in the articular cartilage tissue is deep zone. They collagen in this zone are aligned perpendicularly, its main function is to provide resistance to compressive force which is facilitated by the vertical alignment of collagens [1], [3]. These structural and functional attributes collectively contribute to the vital role of articular cartilage in joint biomechanics.

The tidemark is a three-dimensional undulating structure, serving as a selective membrane that demarcates the mineralized and non-mineralized regions within the OC tissue. It is located in the middle of transition from the soft tissue of articular cartilage to the hard tissue of calcified cartilage, which is called OC interface tissue. The tidemark offers protection against vascular and neural invasion[4] as well as creates a transition zone that enables the transfer of loads at the interface[5], [6]. This structure functions as a protective measure, preventing shearing pressures from affecting the columnar fibers that are connected to the subchondral bone [3], [7]. Collagen fibers/fibrils are notably aligned perpendicular to the tidemark, allowing for smoother stress transmission from the type II collagen-rich articular cartilage to the rigid calcified cartilage, containing type X collagen [8], [9], [10]. While the tidemark is traditionally described as a single layer, its duplication can be attributed to joint development or osteoarthritis [1], [5]. In healthy tissue duplication signifies the progression of the calcification front and may arise from metabolic processes[5]. However, in cartilage degradation and disease, tidemark duplication grows more prominent and are replicated between the spaces where chondrocytes are located[7].

The calcified cartilage region follows the tidemark and is commonly categorized as part of the bone region in osteochondral tissue. In this zone, hypertrophic chondrocytes are found, and collagen is a continuous extension from the deep zone. Blood vessels from the subchondral bone terminate here due to the tidemark blocking their progression. Its primary function is to transfer loads to the underlying bone structure [1]. The cement line is a wavy line that demarcates the calcified region and the subchondral bone and it helps to regulate the amount of nutrient that diffuses from the bone marrow to the articular cartilage [3]. The subchondral bone located below the cement line contains chondrocytes, endothelial cells, stem cells and hydroxyapatite deposit and collagen I. It is the strongest part of the OC tissue; it plays a crucial function in the transmission of force throughout the joint and provides support to the articular cartilage. Studies suggest that about 30% of applied joint load is reduced by the subchondral bone while the cartilage contributes around 2% reduction [11], [12].

1.1.1 Osteochondral Tissue Engineering

The articular cartilage is susceptible to degradation because of wear caused by continuous motion in the joint. This results in the emergence of degenerative disorders such as osteoarthritis. Osteoarthritis (OA) is a highly prevalent form of arthritis characterized by articular cartilage and subchondral bone degeneration. It is also characterized by either complete or partial deterioration of the cartilage tissue [3]. with a global estimate of over 500 million people living with OA according to the world health organization, reports show the statistics increased by about 135% since 1990, a trend expected to increase as the population ages [13].

Over the last two decades they have been varying attempts to regenerate the OC tissue using various tissue engineering approaches. Generally, tissue engineering (TE) involves the use of biomaterial, biomolecule, and cells, to regenerate and or repair tissue. For a successful Regeneration of the OC tissue the different part of the tissue should be considered, hence it is necessary that the scaffolds used mimics the different component of the tissue [14], additionally, when used in vivo the structural integrity of scaffolds should be maintained in relation to the rate of new tissue formation. A key feature of OC regeneration is that the cartilage region is free from vascular and neural invasion as well as infiltration of synovial fluid from the joint[14]. The field of TE has evolved from the use of single layer scaffold to multi layered and gradient scaffolds which is aimed at successfully mimicking the complexity of the tissue however the presence of both the cartilage and subchondral bone layers is essential for the fabrication of osteochondral scaffolds, as these scaffolds consist of heterogeneous layers [11], [15].

1.1.2 Tissue Engineering Techniques for Osteochondral Tissue Regeneration

Osteochondral tissue engineering has witnessed significant advancements in both techniques. and manufacturing processes over the past decade [3] this advancement has facilitated the fabrication of more complex structures that can mimic the tissue. In this study, a combination of electrospinning and 3D bioprinting techniques was employed for scaffold fabrication.

Electrospinning technique is known for its capability of producing fibrous structures with diameters ranging from microns to nanometers. This technique is renowned for producing polymeric nanofibers with various configurations (unimodal, bimodal, aligned, and unaligned). The nanofibers produced are gathered on substrates, creating highly interconnected scaffolds consisting of micro- to non-fibrous structures with a substantial surface area [3].

Electrospinning is widely used in tissue engineering due to its ability to produce fibers closely resembling collagen in native tissue. Successful fabrication of OC scaffolds using electrospinning has been reported. [16] Fabricated a 3D nano porous 5 layered OC scaffold using Electrospinning technique. The scaffolds are composed of materials including gelatin, PCL, and HAP. The results demonstrated that the scaffold had a fibrous structure in each layer, consisting of continuous nanofibers, which facilitated fluids and nutrient transport Additionally by adding HAP to the electrospun scaffold mechanical property of the scaffold increased. However, according to Badami et al. the mechanical properties of layered osteochondral scaffold produced from electrospinning are weaker and possess small pore sizes [17]. However, electrospinning remains versatile technique that has been integrated with other fabrication processes like freeze drying [18] 3D printing [19] to achieve better properties for OC regeneration.

Another often employed method in the regeneration of osteochondral (OC) tissue is Additive Manufacturing (AM) (3D printing). Additive manufacturing techniques account for approximately 80% of scientific articles published since 2018 on the topic of osteochondral regeneration[3]. These techniques have shown success in achieving cell viability, mechanical strength, and a porous structure [20], [21], [22]. Hierarchical layered scaffolds for OC regeneration have been fabricated using 3D printing, scaffolds were reported to support chondrogenic and osteogenic differentiation of human mesenchymal stem cells [23].

Bioprinting relies on selecting the right bioink that is biocompatible, supports cell growth, degrades at a rate like native tissue, and maintains appropriate mechanical properties. Bioinks can be tailored to desired pore sizes [24]. In a study on bone regeneration, Moazzam et al. developed a bioink specifically for bone regeneration The findings of the study indicated that the bioink exhibited remarkable cell vitality, as seen by the high survival rate of cells [25]. Furthermore, the studies claimed that the developed bioink can function as an appropriate foundation for various tissue engineering applications. This served as the basis of the bioink used in this study.

In this study both 3D printing and electrospinning technique were used to fabricate a composite scaffold. The benefit of this technique is that it can be integrated to create a composite scaffold that emulates the inherent osteochondral (OC) structure. The achievement of the graded nature and desirable mechanical properties of the tissue may be facilitated using 3D printing. On the

other hand, the fabrication of nano scale fibers that closely mimic the ECM component of the tidemark can be accomplished by employing the electrospinning technique. Furthermore, considering the structure of the OC tissue; we fabricated a scaffold with both cartilage and subchondral region using gelatin oxidized alginate and HAP. To guide tidemark regeneration and separate both regions a fibrous mesh made of PCL nanofibers was placed in between both Regions.

1.1.3 Biomaterials for Osteochondral Regeneration.

Various biocompatible materials, including natural polymers (e.g., gelatin, alginate, chitosan, silk collagen), synthetic polymers (e.g., polycaprolactone), and metallic polymers, have been employed to fabricate scaffolds for osteochondral tissue [26] . Natural polymers like alginate are recognized for their biocompatibility, degradability, cytocompatibility, and good porosity [27]. Their inherent softness, flexibility, and porous composition facilitates efficient permeation of oxygen and nutrients into their structure, mimicking that of native tissue [28]. Because of their viscoelastic properties alginate have been one of the most sort after natural polymer used in additive manufacturing (bioprinting and bio fabrication) [29]Alginate have been used for cartilage and OC tissue engineering and has been shown to support chondrogenic differentiation[30]. Additional report shows the viability of chondrocyte in alginate[31], [32], [33], [34], [35] According to studies conducted by [32] Alginate gel not only improved chondrogenic expression but also supported the production of collagen II and glycosaminoglycan. However, high molecular weight alginate, typically used for hard tissue, faces challenges in degradation [36] Modifications like sulfation and oxidation can be applied to overcome these issues, improving gel stability and achieving a more physiologically relevant environment [37], [38] Chemical modification of alginate by oxidation process can direct cell function [39], [40], [41]affect degradation. Also, storage modulus and swelling behavior of gels which can be regulated during its oxidation process[42], [43].

Gelatin, a natural polymer, shares compositional similarities with its precursor collagen. Its major advantages include cost-effectiveness, biodegradability, biocompatibility, cell adhesion and differentiation properties, low toxicity, and a porous 3D structure [44], [45]. Gelatin can also undergo enzymatic degradation in the body. Its excellent water absorbability is crucial for tissue regeneration, enhancing nutrient and cell transport within the scaffold [46]. A noticeable disadvantage of gelatin is its thermal instability, as they can change state depending on temperature. Consequently, depending on its application, crosslinking is often necessary.

Synthetic polymers like glutaraldehyde have been used to successfully crosslink gelatin and have exhibited controlled synthesis however one major drawback with method of crosslinking is that it produces cytotoxic materials [47], [48] In addition gelatin has low mechanical strength and is often used in combination with other material or element, one of such is hydroxyapatite (HAP). HAP is a naturally occurring inorganic mineral which has similar composition as bone tissue, and it is commonly used in bone tissue regeneration. incorporating HAP to hydrogels can improve it mechanical property and improve printability of hydrogels and bioactivity of 3D printed scaffold [49], [50]

Synthetic polymers play a crucial role in tissue engineering due to their cost-effectiveness, ease of modification, and adaptability to desired characteristics. Among these, Polycaprolactone (PCL) stands out as a widely utilized synthetic polymer in tissue engineering processes. PCL is a biodegradable, bioabsorbable, and biocompatible polymer known for its high elasticity and durability [51]. The also undergo extended period of degradation about 2 to 3 years when compared to other synthetic polymers like poly-L-lactide (PLLA), poly lactic-glycolic acid (PLGA) and polyglycolic acid (PGA) [52]. PCL also exhibits good viscoelastic properties this makes for ease of fabrication into various forms like nanofibers.

1.2 Problem statement and Hypothesis

Once the articular Cartilage undergoes degeneration, it is unable to heal itself due to the avascular characteristics of the tissue. Clinical procedures, such as mosaicplasty, micro-drilling, autografting, and microfracture among others can be used as treatments for degenerative disorders of the osteochondral (OC) tissue like OA. Nevertheless, these techniques are known to induce vascular invasion, leading to the development of fibrocartilage which has lower mechanical properties when compared to the articular cartilage found in native, healthy tissue. Consequently, it becomes imperative to use a more sustainable strategy to mitigate this issue. Regenerative engineering presents a more promising methodology for the regeneration of osteochondral (OC) tissue, as it aims to replicate the anatomical and physiological characteristics of the tissue. Although studies have shown and fabricated different scaffolds that can aid in regeneration, the full complexity and physiology of the tissue is yet to be successfully mimicked. Additionally, few studies have specifically shown a successful regeneration of the tidemark, nevertheless, the role of tidemark is significant and plays a pivotal role in osteochondral tissue. Notably, the regeneration of the tidemark remains an area with no clearly defined strategy. In this study, it was hypothesized that the interface formed between the layers

of the multilayer graft will possess a thickness of HAP gradient similar to that seen at the native rabbit OC tissue.

1.3 Aim and Objectives

The aim of this study is to fabricate a composite scaffold using 3D bioprinting and electrospinning techniques that can be used for Osteochondral regeneration as well as serve as a strategy for tidemark regeneration.

Objectives

- To fabricate composite scaffold grafts using 3D bioprinter and electrospinning
- To evaluate and characterize native tissue and fabricated scaffold (mechanical test, mineral distribution)
- To create mineral gradient across the interface.

Chapter 2 - Materials and methods

2.1 Materials

Hydroxyapatite (677418-10G Sigma-Aldrich), polycaprolactone MW = 80000 g/mol (440744 Sigma-Aldrich), Acetic acid (695092 Sigma-Aldrich), pyridine (270970 Sigma-Aldrich), formic acid (1.10854 Sigma-Aldrich), glutardialdehyde (Nr-4995.1 Roth), β-glycerophosphate disodium salt hydrate (G9422-50G Sigma-Aldrich), Glycine (1610718 Bio-Rad), Ethylene glycol (324558-1L Sigma-Aldrich), Phosphate buffer salt (Sigma-Aldrich), Formalin (HT501128-4L Sigma-Aldrich), sodium periodate (S-1878 Sigma -Aldrich).

2.2 Mesh fabrication by electrospinning

To produce nanofiber mesh 8wt% of PCL was dissolved in 0.05ml of formic acid and acetic acid, and 0.006ml of pyridine. The solution was stirred for 2 hours at 40^{o}C. The solution was loaded into a 6ml syringe with 21G blunt tip and electrospun for 10 hours at 9kv at a distance 7cm from the tip of the needle to the collecting plate. The fibrous layer was then allowed to dry at room temperature for 24hours before cutting into the required shape.

2.3 Bioink preparation

The overall procedure is described in Figure 2. First oxidized alginate was synthesized following the procedures outlined in [25]. Briefly 1.8g of Sodium alginate was dissolve with DI water at room temperature until completely dissolved. A total of 0.18g of sodium periodate was then added to the alginate solution and stirred for 1hour under dark conditions to obtain oxidized alginate (OXA). To terminate the oxidation process 0.25 mL of Ethylene glycol was added to the solution and stirred for 30mins. The resultant solution was subsequently transferred into a dialysis membrane with a 15 kDa molecular weight cut-off, solution under dialysis for 24 hours Fourier transform infrared (FTIR) analysis was conducted to verify the oxidation of alginate (Nicolet iS10, Thermo Scientific). The pure stock solution was stored at 4°C until use.

HAP was added to the bioink previously prepared as described above for the bone region (bottom layer) of the OC graft. To prepare this bioink, first 1ml of OXA (aqueous solution) was mixed with 0.4ml of DI water in a tube. Then, 0.018g of HAP and 0.15g of β-glycerophosphate disodium salt hydrate were added to the (OXA + DI Water). The solution was vortexed for 30

seconds. To the prepared solution, 1ml of 12%w/v gelatine (aqueous solution) is added and vortexed to obtain a homogenous solution. For the cartilage region (top layer) of the graft, the 12%w/v of gelatine (aqueous solution) and OXA (aqueous solution) was mixed in the ratio 1:1.

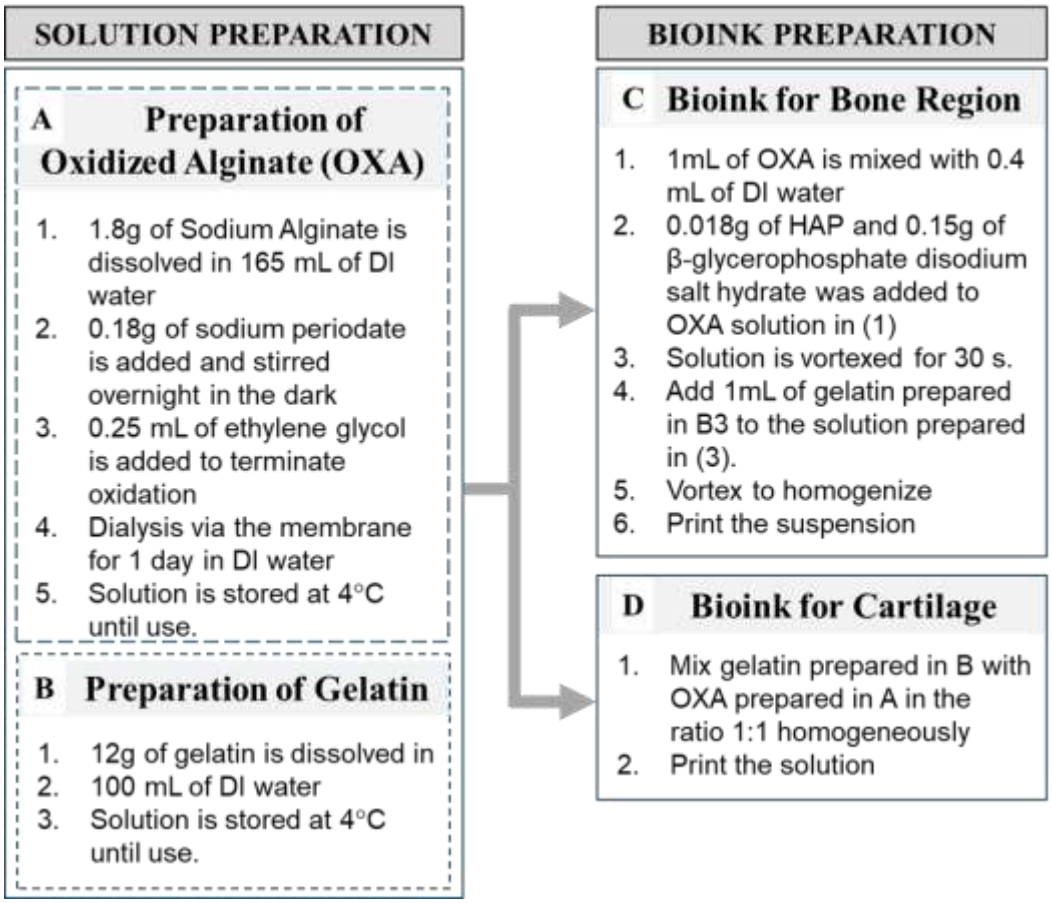

Figure 2: Bioink preparation for the printing of osteochondral

2.4 Fabrication of composite OC grafts

To fabricate our multilayer bioprinted composite scaffold, first, the prepared hydrogels were placed into separate syringes and degassed for 30 seconds to get rid of the air bubbles in the syringe. It was then transferred to an ice bath for 30 seconds and placed into the printing cartridge. The grafts were printed with BioX 3D printer (CELLINK, Goteborg, Sweden) using a temperature-controlled printhead and printing stage to ensure good printability conditions. First, the bottom layer (bone region) of the graft was printed using the bioink for the bone region (Figure 1C). For the implantation of the fibrous mesh representing the tidemark, the PCL membrane was immersed in a gelatine solution for a few seconds until the surface of the membrane was completely coated, and the coated membrane was placed on the printed bottom

layer of the graft. The top layer (cartilage region) was immediately printed over the mesh using a 27G nozzle. The overall printing process is shown in Figure 3.

After printing, the grafts were left to undergo cryogelation for 24 hours at -20ºC and then crosslinked in a 1% glutaraldehyde solution for 2 hours. To neutralize the aldehyde group, the printed grafts were treated with 2%w/v glycine for 1 hour, followed by washing in DI water up to 10 times. They were then immersed in a 0.2%w/v solution of sodium borohydride for 2 hours, finally washed thoroughly up to 10 times with PBS, and lyophilized for further use.

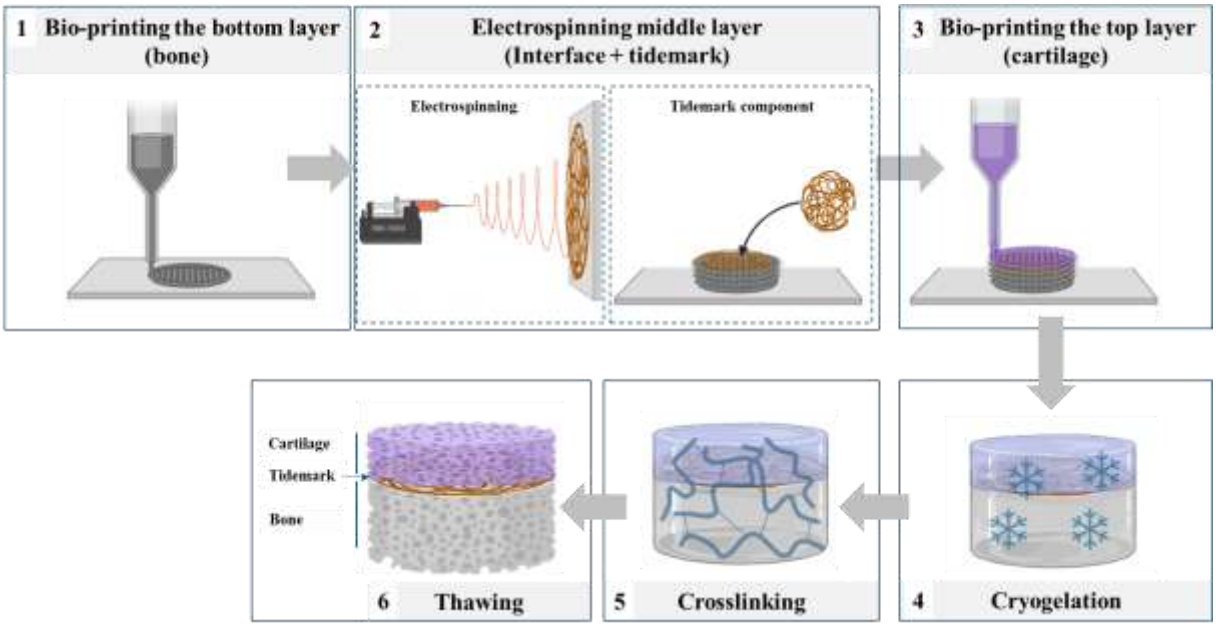

Figure 3: Fabrication of Composite Multilayer Osteochondral Graft

2.5 Rheological and thermogravimetric analysis of hydrogel

An oscillatory test (Anton Paar, MCR302, Graz, Austria) was performed for bioinks using two 50mm parallel plates to examine temperature dependence of the storage modulus (G') and loss modulus (G") for temperatures between 10 and 40°C (n=3/group). The experiment was conducted at a heating rate of 1□C/min, frequency of 1 Hz, and shear strain of 1%. The shear-dependent viscosities of the bioinks were characterized using a strain sweep test at a rate from 0.1 to 100 1/s (n=3/group). Thermogravimetric analysis (Netzsch DSC-TGA, Selb, Germany) was performed on both Bioinks by heating up to 500oC from room temperature at 25oC/min (n=3/group).

2.6 Pore diameter and fiber diameter distribution

Pore diameters and fiber diameters of the specimens were measured using Image-J (NIH, USA) as described previously[53], [54]. Briefly, ten equally distanced lines were marked on the SEM micrographs, and the diameters of fibers overlapping with the lines were measured. The same procedure was followed to measure the diameter of the pores.

2.7 Swelling and Degradation test

The freeze-dried scaffolds were first weighed to establish their dry weight W(o), and then the scaffolds were immersed in a 10mM PBS solution 24 hours. The swollen scaffolds were retrieved at different time points (5hour and 24 hour) and weighed to obtain their final mass. For this test n=3 and average were calculated. The swelling capacity was quantified using the equation:

$$Swelling\ capacity\ (\%) = \frac{W(f)-W(o)}{W(f)} \times 100$$

For degradation analysis, initial mass W(o) was determined by weighing dried scaffolds. Then Scaffolds were immersed in PBS solution and incubated at 37^{o}C with 5% CO2 for 21 days. At various timepoints (1, 7, 14, and 21 days), 3 scaffolds each were retrieved and washed with DI water to remove any residual PBS. Then Scaffolds were lyophilized overnight and then weighed to determine final weight W(f). The degradation rate was obtained using the equation.

$$\text{degradation rate } (\%) = \frac{W(o)-W(f)}{W(o)} \times 100$$

2.8 Compression Test

The rabbits (8-10 month-old male) were obtained from a local abattoir, and the knee joints were harvested to create cylindrical plugs (from the femoral bone) with dimensions of 3mmx3mm (diameter x height). The specimens of the OC tissue and the grafts were compressed using TA.XTplusC texture analyzer (Stable Micro Systems, U. K.) at a cross-head speed of 3mm/min until complete deformation (n=5/group). The stress-strain curve and load compression curve were plotted from the data obtained.

2.9 Scaffold/Tissue Morphology and EDX analysis

The fiber diameter and pore diameter distribution of the PCL mesh, as well as the morphology of the grafts and native OC tissue, were observed using scanning electron microscopy (SEM, JSM-IT200, JEOL). The specimens were coated with gold using the sputter coater

(turbomolecular pumped coater Q150T, Quorum Technologies, East Sussex, UK) and examined at accelerating voltages of 10kV and 5kV for PCL mesh and grafts, respectively, with a probe current of 40pA. To prepare the osteochondral tissue for imaging, samples collected from rabbit knee joints were placed in saline solution for 2 hours at 4^{o}C and then fixed in 10%formalin overnight. The samples were further dehydrated in a graded ethanol series and then dried before use. An EDX evaluation was performed on the grafts and tissues to determine the mineral presence and distribution using the same instrument. An accelerating voltage of 20kV and a probe current of 60pA were used for the analysis.

2.10 Micro-CT Analysis

Fresh osteochondral tissue plugs were harvested from rabbit knee joints and tested immediately. Since scanning takes several hours depending on the required resolution, the specimens were kept hydrated during scan using a custom made chamber. The specimens were scanned using a micro-CT machine (SkyScan 1272 micro-CT, Bruker, Billerica, MA, USA) with a voltage of 60kV, current of 60uA, binning of 2×2, total time of 16hrs, and Al filter of 0.5mm. A 3D image reconstruction and bone mineral density (BMD) analysis were done using CVox and CTAn, respectively (Bruker Micro-CT 3D-Suite).

2.11 Statistical Analysis

The swelling of the composite graft after 5hrs and 24hrs, as well as the mechanical performance of the grafts and the native tissue, were compared using a t-test, and significance was achieved for $p<0.05$.

Chapter 3 - Results

3.1 Rheology and Thermogravimetric analysis of the bioinks

Rheological analysis was conducted to assess the shear thinning properties and printability of the gels (Figure 4A, B). The gelation points, where the storage modulus equals the loss modulus, were determined as 28.7°C and 29.7°C, respectively, for the bottom layer (bone region containing Gel+OXA+HAP) and the top layer (cartilage region containing Gel+OXA). Below 28.7°C, both inks exhibited viscoelastic properties with dominating elastic behavior (storage modulus > loss modulus). Additionally, analysis of the hydrogel viscosity under varying shear rates revealed shear thinning properties. As the shear rate increased, the viscosity of the inks decreased, indicating favorable characteristics for a 3D extrusion printing.

The TGA performed on both hydrogel bioinks verified the presence of HAP in the ink representing the bone region. In Figure 4C, the weight of both materials exhibited an immediate weight reduction around 100°C attributed to water evaporation. When the temperature reached 500°C, the remaining weight of the cartilage region (Gel+OXA) decreased to 1.62±0.06%. In contrast, the bioink representing the bone region (Gel+OXA+HAP) retained its weight of 5.11±0.08%. The difference between the average values is 3.49% and gives us the remaining percentage of non-decomposing components (HAP, β-glycerophosphate disodium salt hydrate, and polymers) at 500°C in the ink for bone region. The percentage of HAP as calculated from the raw materials (Figure 1) is 0.70%. The bone and cartilage parts of the native OC tissue had a non-decomposing material content of 48.4±1.2% and 4.94±0.72% at 500°C, respectively (Figure 4D).

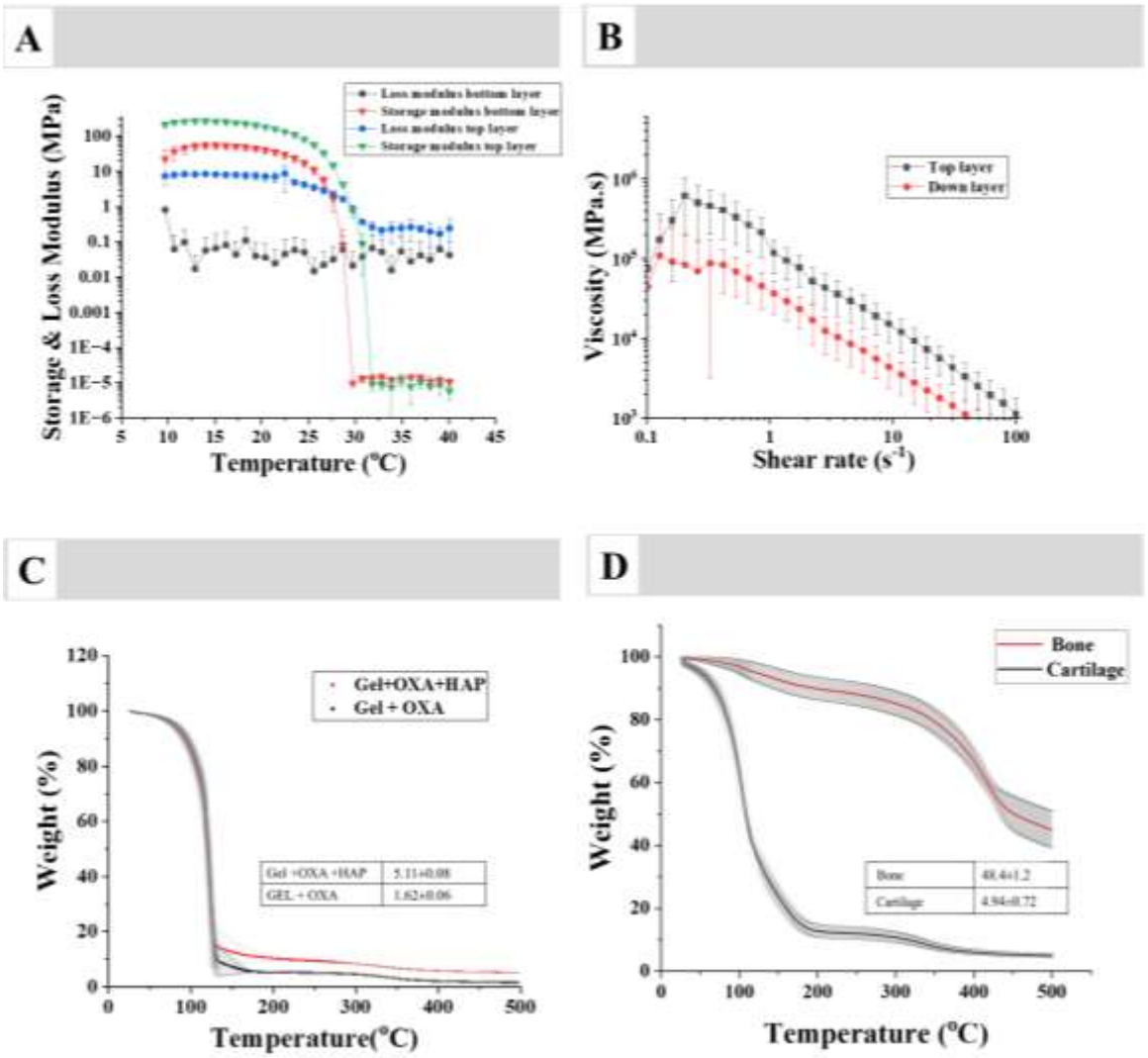

Figure 4: Characterization of bioinks and the OC tissue (n=3/group, error bars denote STD). (A) Temperature dependence of storage and loss moduli, (B) shear dependence of viscosity, TGA analysis, (C) for determining the HA content in the composite graft, and (D) mineral content of native tissue.

3.2 physiological characterization of composite graft

SEM micrographs shown in figure 5A and 5C reveal interconnected porous structure of the grafts while randomly aligned fibres can be seen in figure 5B.The top layer of the scaffold representing the cartilage region had pores with sizes ranging from 50µm to 400µm, while the bone region had pore sizes ranging from 40µm to 500µm, as shown in Figure 4D and 4F.. The electrospun PCL mesh used as the tidemark region has a fibre diameter ranging from and a pore from about 0.1µm to 0.7µm (figure 5E).

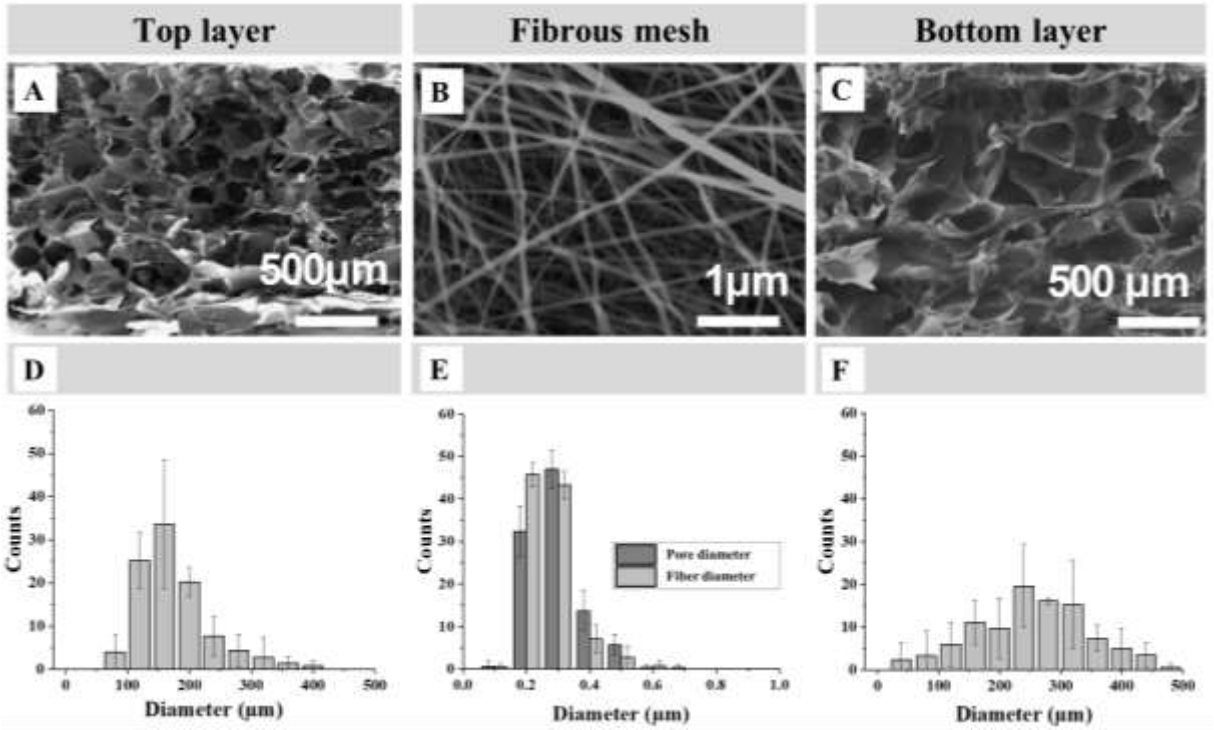

Figure 5: SEM micrographs depicting morphological structure of the layers of composite graft and electrospun mesh representing the tidemark. (A) SEM micrograph of the top layer (representing cartilage region, Gel+OXA), (B) SEM micrograph of fibrous mesh representing the tidemark, (C) SEM micrograph of bottom layer (representing the bone region, Gel + OXA+ H2O+ β-GP+HAP), (D-F) pore diameter distribution of top layer, fibrous mesh and bottom layer, and (E) diameter distribution of PCL fibers. Error bars represent standard deviation (n=3/group).

3.3 Oxidation of alginate, swelling and degradation of grafts

Composite grafts were subjected to swelling and degradation tests for 24 hours and 21 days, respectively (Figure 6). Results of the swelling test showed that grafts swelled (absorbed water) by 654% and 633% after 5 hours and 24 hours of incubation time, respectively (no significant difference, $p>0.05$). Figure 6B demonstrates the degradation of composite grafts for a period of 21days. Overall, more than 25% of the graft degraded after 21 days. Oxidation of the alginate was verified with a characteristic aldehyde peak seen at 1734.7 1/cm (Figure 6C).

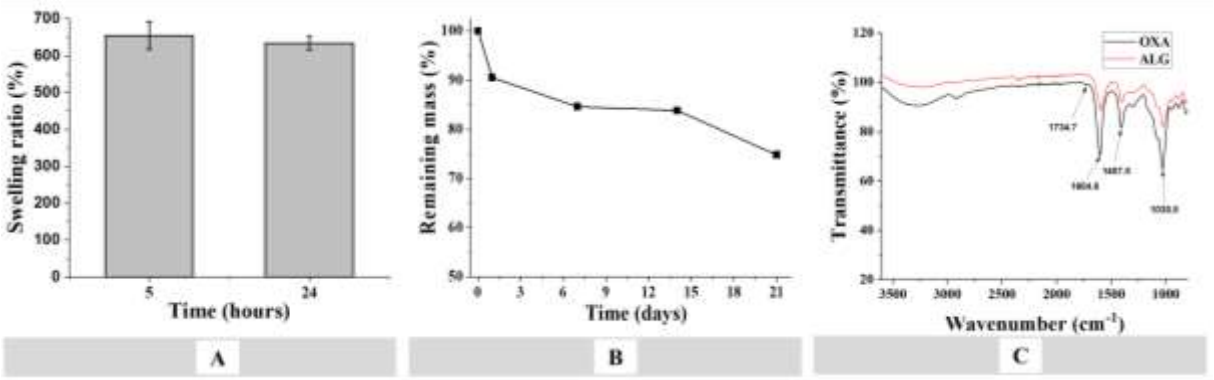

Figure 6: : (A) Swelling test result and (B) degradation rate of composite grafts, and FTIR characterization of the bioinks. Error bars indicate standard deviation (n=3).

3.4. Mechanical characterization

Compression tests were carried out on composite grafts and OC tissues harvested from the knee joint of rabbits. As depicted in Figure 7A&C, the stress-strain response of the native OC tissue exhibited a capacity to endure a compressive stress of 24.4±3.9MPa when strained to 14.4±0.03%, whereas the graft could withstand a stress of 2.7±1.8MPa. Notably, the grafts sustained a longer strain, reaching an ultimate value of 37.3±3.8%. Moduli of the native OC tissue and the graft were found as 1.8±0.1MPa and 0.07±0.05MPa, respectively. For load-compression characteristics, as illustrated in Figure 7B&C, a load of 37.4±6.3N was needed to compress the OC tissue by 0.6mm. Similarly, the graft was subjected to a load of 21.0±9.0N when compressed by 2.6mm for complete deformation. The stiffness values of the OC tissue and the graft were 83.3±1.9N/mm and 5.60±2.85N/mm, respectively. The cross-sectional area of the OC tissue specimens and the grafts were measured as 1.81±0.06mm^2 and 6.57±0.82mm^2, respectively.

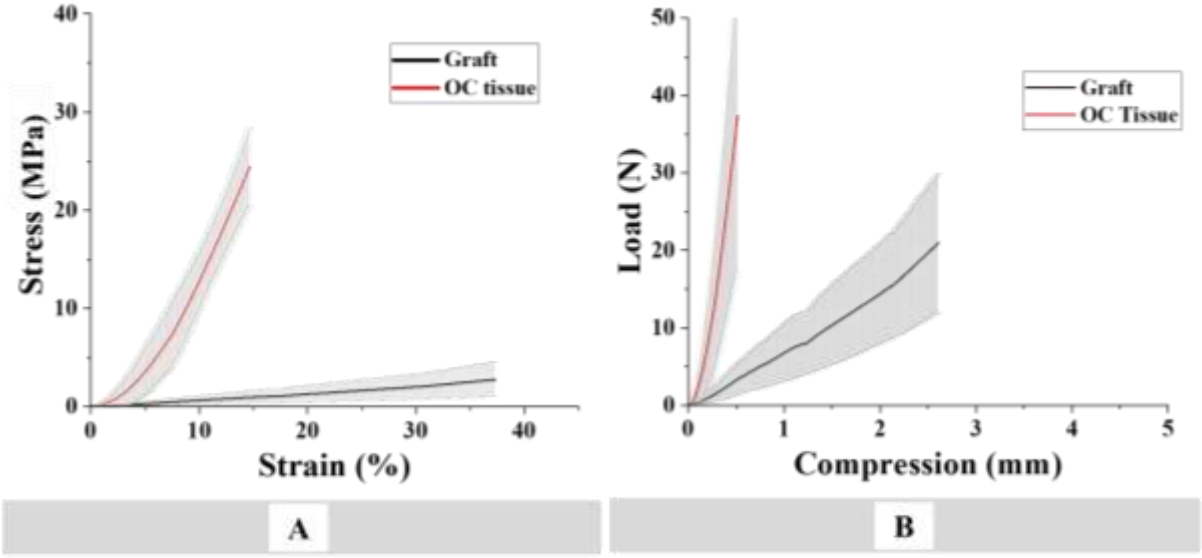

C

	Stress at Break (MPa)	Strain at Break (%)	Modulus (MPa)	Stiffness (N/mm)	Load at Break (N)	Strain at Break (mm)
OC Tissue	24.4±3.9*	14.4±0.03*	1.8±0.1*	83.3±1.9*	37.4±6.3*	0.6±0.0*
Graft	2.7±1.8	37.3±3.8	0.07±0.05	5.60±2.85	21.0 ±9.0	2.6 ±0.0

* Difference at p<0.05

Figure 7: Mechanical characterization. (A) stress-strain curve, (B) Load compression graph, and (C) The corresponding values of the key properties. Shaded regions represent error bars (error bars = standard deviation).

3.5 Mineral presence and distribution

Mineral presence and distribution were determined using EDX mapping and micro-CT analysis. Macroscopic observation of the OC tissue (Figure 8A1) or SEM image (Figure 8A3) are informative but not sufficient to claim the presence of minerals. EDX elemental mapping of native tissue for phosphorous (P) and calcium (Ca) showed the presence of minerals in the bone region, while no mineral presence was visualized in the cartilage region (Figure 8A2). Similarly, the gross observation of the 3D printed OC graft (Figure 8B1) and its SEM micrograph (Figure 8B3&4) show different layers; however, do not provide data for the presence of minerals. Its elemental mapping, on the other hand, showed mineral presence in the bone region, with no minerals in the cartilage region (Figure 8B2).

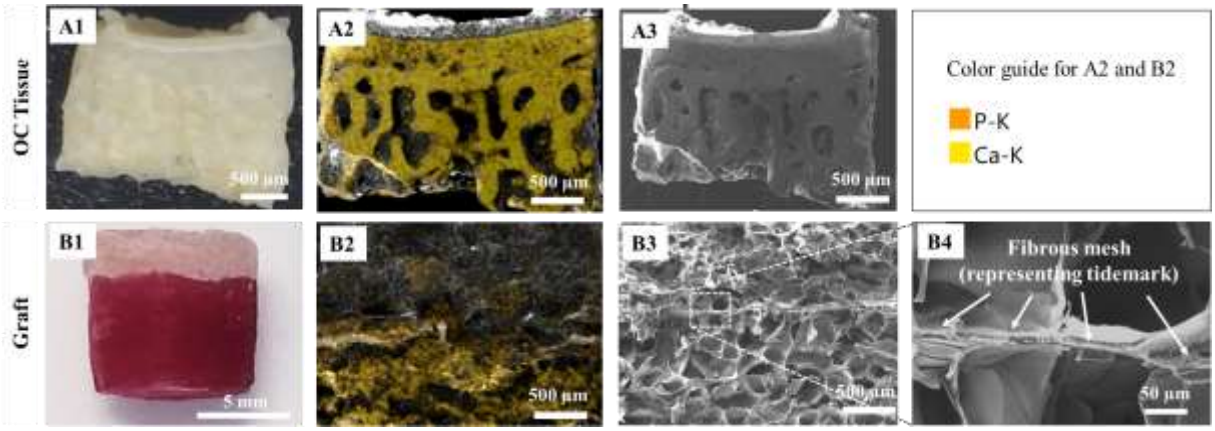

Figure 8: Mineral presence and distribution in the OC tissue and grafts. (A1, B1) optical images, (A2, B2) EDX elemental mapping, and (A3, B3) SEM micrographs of native OC tissue and composite graft. (B4) magnified image of the interface between the layers. P: phosphorous and Ca: calcium for A2 and B2.

Reconstructed micro-CT images of the graft (Figure 9A) and native OC tissue (Figure 9B) showed a structural similarity. They both had a cartilage region on the top, an interface, and a bone region at the bottom. Visually and qualitatively, it is possible to differentiate the layers of cartilage and bone for both native OC tissue and graft as depicted in Figure 9A-C. However, in this study, the aim was to create a gradient of minerals in the graft to mimic the mineral distribution observed in the native OC tissue. It is seen in Figure 9D that the BMD, i.e., mineral concentration, is increasing as traveled from top (adjacent to cartilage) to bottom (adjacent to bone), as expected. The mineral density plateaued at both ends, while a gradual change was observed within the interface region. The thickness of gradient of the mineral concentration was found as 151µm. It should be noted that the mineral concentration does not represent the actual amount of mineral content because the instrument was not calibrated for this purpose. The native OC tissue possessed higher mineral density (ranging between 4.44±1.44 and 17.98±5.85) as compared to the graft (ranging between 1.80±0.17 and 2.86±0.16) as shown in Figure 9D&E. The lower mineral content characterized in the graft is due to the processing capacity of the 3D bioprinter.

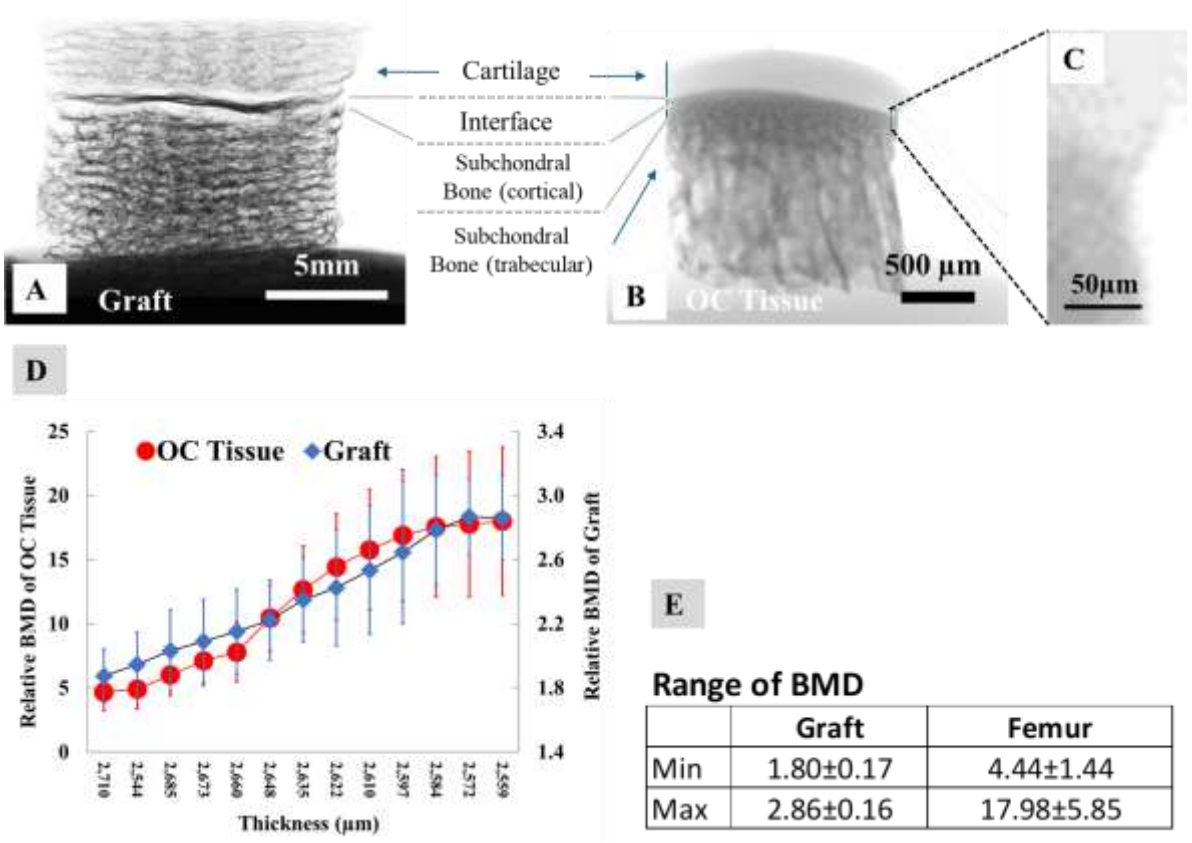

	Graft	Femur
Min	1.80±0.17	4.44±1.44
Max	2.86±0.16	17.98±5.85

Figure 9: Mineral presence and distribution in the OC tissue and grafts. (A1, B1) optical images, (A2, B2) EDX elemental mapping, and (A3, B3) SEM micrographs of native OC tissue and composite graft. (B4) magnified image of the interface between the layers. P: phosphorous and Ca: calcium for A2 and B2.

Chapter 4 - Discussion

The intricate nature of the native OC tissue poses challenges in fabricating scaffolds that accurately replicate its structure. Despite the pivotal role of the tidemark within OC tissue, this component of the tissue has been inadequately addressed in over ninety percent of studies published in the past decade, and successful regeneration of the tidemark component remains unreported[1], [8]. In this study, our main objective was to design and fabricate a graft that can closely mimic the distance of the gradient of minerals and the tidemark seen in the native tissue. To achieve this, graft for OC tissue were fabricated using two distinct hydrogel compositions for each tissue region (bone and cartilage). The hydrogels employed consisted of gelatine+OXA for the cartilage region and gelatine+OXA+HAP for the bone region. To replicate the structure of the tidemark, an electrospun polycaprolactone (PCL) membrane was placed between two 3D bioprinted grafts representing the cartilage and bone regions.

The gelation points and printability of both hydrogels was initially assessed through rheological analysis. As depicted in Figure 4A, it was observed that around 29°C, the storage modulus equaled the loss modulus in both hydrogels, indicating a similar gelation point for both materials. The addition of hydroxyapatite (HAP) to the hydrogel for the bone region did not significantly alter its gelation properties. Also, hydrogel when subjected to shear stress exhibited a non-Newtonian behavior. As seen in Figure 4B, shear rate increases with decrease in velocity. This behavior suggests that hydrogel can be extruded from the nozzle and upon pressure release printed shape can be maintained. Suggesting their suitability for smooth extrusion in 3D printing applications [55].

A TGA analysis was conducted on the bioinks to validate the presence of HAP in the composite scaffold. TGA is a very convenient method to determine the mineral content in native tissues as well as in the mineralized structures because minerals, including hydroxyapatite, still remain in the structure when heated up to 500°C, a temperature at which most of the organic materials fully decompose[56], [57]. In this study, the TGA verified the presence of around 3.49% undecomposed material, which is mostly HAP and β-glycerophosphate disodium salt hydrate. Considering the negligible decomposition of HAP and around 45% by weight decomposition of the latter at 500°C[56], calculations based on the formulation of the Gel+OXA+HAP bioink yielded a value of 3.62% remaining undecomposed material, which is close to 3.49% determined by TGA analysis.

As indicated in figure 5, SEM micrographs showed porous interconnected scaffolds with varying pore sizes. The top layer representing the cartilage region had smaller pores with peak diameter of 160µm compared the bone region with 250µm. Although similar compositions were used for both regions the difference in the pore size can be attributed to the presence of DI water in the hydrogel composition used in the down layer that formed pores upon freeze-drying. The porosity of the electrospun fiber was shown to be between 0.1µm to 0.7µm. The tidemark in native tissue not only serves to a region that separates calcified and uncalcified cartilage but also functions as a barrier against the invasion of blood vessels into the uncalcified cartilage region. This property aligns with one of the key characteristics of articular cartilage found in osteochondral (OC) tissue. Due to the small size of the pores in the electrospun fiber, scaffolds can effectively prevent blood vessel penetration in vivo. This characteristic enables the scaffold to function as the tidemark in vivo, facilitating the formation of articular cartilage rather than fibrocartilage, which typically results from blood vessel infiltration into the cartilage[1].

The grafts fabricated in this study swelled within the first 5 hours and maintained their behavior for 24 hours. This demonstrates the potential of the grafts to be used as filler grafts for OC defects. As commonly accepted by the orthopedics community, a significant challenge with the use of grafts in OC defects is the formation of an interface between the graft and the host tissue due to poor biological integration [58]. Therefore, swelling of the hydrogel upon its insertion into the defect size may improve the integration between the graft and the host tissue by applying pressure onto the layer of connection

The degradation test conducted revealed that scaffolds maintained its integrity after 21 days of immersion in PBS and around 75% of grafts remained ed intact after 21 days of test. This result suggests that the use of oxidized alginate helped reduce the degradation of the hydrogel and that grafts can be safely and appropriately used for in vivo applications to maintain the integrity of the structure during tissue regeneration. A previous work investigated the oxidation of alginate to modify the degradation rate of alginate-based bioinks for cartilage tissue engineering applications[59]he rate of degradation was found to be highly dependent on the oxidation level of the bioink. The study also reported that the initially printed geometry was maintained throughout a 4-week in vitro culture period.

When subjected to compression test, the grafts exhibited inferior mechanical resistance as compared to the native tissue in terms of stress, modulus, load and stiffness. Despite this poor

performance of the grafts, it is still possible to claim the suitability of the grafts for the intended application because implantation of the graft to the defect site in vivo would eventually result graft's invasion by the host cells from the respective zones of the OC interface. The cells would then synthesize the ECM components to improve the mechanical properties as the tissue regenerates.

To evaluate the mineral presence and distribution across the interface from cartilage to bone, EDX and micro-CT scans were performed on osteochondral tissue from the femur and the constructed osteochondral graft. As depicted in Figure 9, the cartilage region of the graft was free of minerals, while the bone region was stained for the presence of P and Ca (Figure 9B2). This characteristic of the graft was similar to that of the native OC tissue (Figure 9A2). In addition, the electrospun mesh placed to serve as the tidemark was clearly evident at the interface between cartilage and bone regions of the graft (Figure 9B3&4). To have a closer look at the change of mineral (HAP) concentration as a function of thickness from cartilage to bone, a micro-CT scan was performed on the native OC tissue and the graft. As shown in Figure 8, the distance of the gradient of mineral concentration in the graft was similar to that seen in the native OC tissue. Both specimens exhibited a thickness gradient of 151µm. The mineral concentration plateaued at both ends of the curve of the gradient, indicating a constant mineral content for bone and no mineral for cartilage (if the instrument readings were calibrated based on the mineral content of the cartilage). The mineral distribution achieved in the graft suggests that the graft has the potential to support simultaneous osteogenic and chondrogenic activities both in vitro and in vivo. Creating a gradient of mineral concentration in scaffolds/grafts to mimic the change of minerals in the native OC tissue has been previously attempted by different research groups [1], including us [60]. However, a physiologically relevant thickness gradient of mineral concentration with this precision has not been achieved in a controlled manner. Therefore, the results of this study are expected to significantly contribute to the orthopedic-related research efforts to find a solution to a disease affecting around 250 million people over the age of 50, worldwide.

Chapter 5 - Conclusion

The OC graft fabricated using combined bioprinting and electrospinning techniques demonstrated a potential to serve as a biomimetic hydrogel filler for regenerating OC defects to restore the function of the knee joint. A physiologically relevant thickness gradient of mineral concentration with high precision has been achieved in a controlled manner. It is expected that the proposed osteochondral graft will be effectively used to address a significant clinical problem that affects millions of people worldwide, with significant societal and economic impacts.

References

[1] N. Yildirim, A. Amanzhanova, G. Kulzhanova, F. Mukasheva, and C. Erisken, “Osteochondral Interface: Regenerative Engineering and Challenges,” *ACS Biomater Sci Eng*, vol. 9, no. 3, pp. 1205–1223, Mar. 2023, doi: 10.1021/acsbiomaterials.2c01321.

[2] P. Morouço, C. Fernandes, and W. Lattanzi, “Challenges and Innovations in Osteochondral Regeneration: Insights from Biology and Inputs from Bioengineering toward the Optimization of Tissue Engineering Strategies,” *J Funct Biomater*, vol. 12, no. 1, Mar. 2021, doi: 10.3390/JFB12010017.

[3] S. Barui, D. Ghosh, and C. T. Laurencin, “Osteochondral regenerative engineering: Challenges, state-of-the-art and translational perspectives,” *Regenerative Biomaterials*, vol. 10. Oxford University Press, 2023. doi: 10.1093/rb/rbac109.

[4] C. Deng, C. Xu, Q. Zhou, and Y. Cheng, “Advances of nanotechnology in osteochondral regeneration,” *Wiley Interdiscip Rev Nanomed Nanobiotechnol*, vol. 11, no. 6, Nov. 2019, doi: 10.1002/WNAN.1576.

[5] M. Kazemi and J. L. Williams, “Properties of Cartilage–Subchondral Bone Junctions: A Narrative Review with Specific Focus on the Growth Plate,” *Cartilage*, vol. 13, no. 2. SAGE Publications Inc., pp. 16S-33S, Dec. 01, 2021. doi: 10.1177/1947603520924776.

[6] C. B. Carballo, Y. Nakagawa, I. Sekiya, and S. A. Rodeo, “Basic Science of Articular Cartilage,” *Clin Sports Med*, vol. 36, no. 3, pp. 413–425, Jul. 2017, doi: 10.1016/J.CSM.2017.02.001.

[7] R. Chen, S. Chen, X. M. Chen, and X. Long, “Study of the tidemark in human mandibular condylar cartilage,” *Arch Oral Biol*, vol. 56, no. 11, pp. 1390–1397, Nov. 2011, doi: 10.1016/J.ARCHORALBIO.2011.04.007.

[8] J. C. Mansfield and C. Peter Winlove, “A multi-modal multiphoton investigation of microstructure in the deep zone and calcified cartilage,” *J Anat*, vol. 220, no. 4, p. 405, Apr. 2012, doi: 10.1111/J.1469-7580.2012.01479.X.

[9] A. Thambyah and N. Broom, “On how degeneration influences load-bearing in the cartilage–bone system: a microstructural and micromechanical study,” *Osteoarthritis Cartilage*, vol. 15, no. 12, pp. 1410–1423, Dec. 2007, doi: 10.1016/J.JOCA.2007.05.006.

[10] I. Redler, V. C. Mow, M. L. Zimny, and J. Mansell, “The ultrastructure and biomechanical significance of the tidemark of articular cartilage.,” *Clin Orthop*

Relat Res, vol. 112, pp. 357–362, 1975, doi: 10.1097/00003086-197510000-00038.

[11] H. Madry, C. N. van Dijk, and M. Mueller-Gerbl, “The basic science of the subchondral bone,” *Knee Surg Sports Traumatol Arthrosc*, vol. 18, no. 4, pp. 419–433, Apr. 2010, doi: 10.1007/S00167-010-1054-Z.

[12] M. Tamaddon, L. Wang, Z. Liu, and C. Liu, “Osteochondral tissue repair in osteoarthritic joints: clinical challenges and opportunities in tissue engineering,” *Biodes Manuf*, vol. 1, no. 2, pp. 101–114, Jun. 2018, doi: 10.1007/S42242-018-0015-0.

[13] “Osteoarthritis,” World Health Organization. Accessed: Feb. 02, 2024. [Online]. Available: https://www.who.int/news-room/fact-sheets/detail/osteoarthritis

[14] S. Khorshidi and A. Karkhaneh, “A review on gradient hydrogel/fiber scaffolds for osteochondral regeneration,” *J Tissue Eng Regen Med*, vol. 12, no. 4, pp. e1974–e1990, Apr. 2018, doi: 10.1002/TERM.2628.

[15] R. F. Canadas, A. P. Marques, R. L. Reis, and J. M. Oliveira, “Osteochondral Tissue Engineering and Regenerative Strategies,” *Studies in Mechanobiology, Tissue Engineering and Biomaterials*, vol. 21, pp. 213–233, 2017, doi: 10.1007/978-3-319-44785-8_11.

[16] F. Hejazi, S. Bagheri-Khoulenjani, N. Olov, D. Zeini, A. Solouk, and H. Mirzadeh, “Fabrication of nanocomposite/nanofibrous functionally graded biomimetic scaffolds for osteochondral tissue regeneration,” *J Biomed Mater Res A*, vol. 109, no. 9, pp. 1657–1669, Sep. 2021, doi: 10.1002/JBM.A.37161.

[17] A. S. Badami, M. R. Kreke, M. S. Thompson, J. S. Riffle, and A. S. Goldstein, “Effect of fiber diameter on spreading, proliferation, and differentiation of osteoblastic cells on electrospun poly(lactic acid) substrates,” *Biomaterials*, vol. 27, no. 4, pp. 596–606, Feb. 2006, doi: 10.1016/J.BIOMATERIALS.2005.05.084.

[18] S. Zhang *et al.*, “Bi-layer collagen/microporous electrospun nanofiber scaffold improves the osteochondral regeneration,” *Acta Biomater*, vol. 9, no. 7, pp. 7236–7247, 2013, doi: 10.1016/J.ACTBIO.2013.04.003.

[19] W. He *et al.*, “Integrating coaxial electrospinning and 3D printing technologies for the development of biphasic porous scaffolds enabling spatiotemporal control in tumor ablation and osteochondral regeneration,” *Bioact Mater*, vol. 34, pp. 338–353, Apr. 2024, doi: 10.1016/J.BIOACTMAT.2023.12.020.

[20] M. Kesti *et al.*, “Bioprinting Complex Cartilaginous Structures with Clinically Compliant Biomaterials,” *Adv Funct Mater*, vol. 25, no. 48, pp. 7406–7417, Dec. 2015, doi: 10.1002/ADFM.201503423.

[21] R. Levato *et al.*, “The bio in the ink: cartilage regeneration with bioprintable hydrogels and articular cartilage-derived progenitor cells,” *Acta Biomater*, vol. 61, pp. 41–53, Oct. 2017, doi: 10.1016/J.ACTBIO.2017.08.005.

[22] X. Cui, K. Breitenkamp, M. G. Finn, M. Lotz, and D. D. D’Lima, “Direct Human Cartilage Repair Using Three-Dimensional Bioprinting Technology,” *https://home.liebertpub.com/tea*, vol. 18, no. 11–12, pp. 1304–1312, Apr. 2012, doi: 10.1089/TEN.TEA.2011.0543.

[23] X. Zhou *et al.*, “3D Printed scaffolds with hierarchical biomimetic structure for osteochondral regeneration,” *Nanotechnology, Biology, and Medicine*, vol. 19, pp. 58–70, 2019, doi: 10.1016/j.nano.2019.04.002.

[24] S. H. Park, C. S. Jung, and B. H. Min, “Advances in three-dimensional bioprinting for hard tissue engineering,” *Tissue Eng Regen Med*, vol. 13, no. 6, pp. 622–635, Dec. 2016, doi: 10.1007/S13770-016-0145-4/METRICS.

[25] M. Moazzam *et al.*, “Macroporous 3D printed structures for regenerative medicine applications,” *Bioprinting*, vol. 28, no. November, p. e00254, 2022, doi: 10.1016/j.bprint.2022.e00254.

[26] B. Zhang, J. Huang, and R. J. Narayan, “Gradient scaffolds for osteochondral tissue engineering and regeneration,” *J Mater Chem B*, vol. 8, no. 36, pp. 8149–8170, Sep. 2020, doi: 10.1039/D0TB00688B.

[27] A. C. Hernández-González, L. Téllez-Jurado, and L. M. Rodríguez-Lorenzo, “Alginate hydrogels for bone tissue engineering, from injectables to bioprinting: A review,” *Carbohydrate Polymers*, vol. 229. Elsevier Ltd, Feb. 01, 2020. doi: 10.1016/j.carbpol.2019.115514.

[28] S. J. Buwalda, K. W. M. Boere, P. J. Dijkstra, J. Feijen, T. Vermonden, and W. E. Hennink, “Hydrogels in a historical perspective: From simple networks to smart materials,” *Journal of Controlled Release*, vol. 190, pp. 254–273, Sep. 2014, doi: 10.1016/J.JCONREL.2014.03.052.

[29] J. Groll *et al.*, “Biofabrication: reappraising the definition of an evolving field,” *Biofabrication*, vol. 8, no. 1, p. 013001, Jan. 2016, doi: 10.1088/1758-5090/8/1/013001.

[30] K. Ma, A. L. Titan, M. Stafford, C. H. Zheng, and M. E. Levenston, “Variations in chondrogenesis of human bone marrow-derived mesenchymal stem cells in

fibrin/alginate blended hydrogels," *Acta Biomater*, vol. 8, no. 10, pp. 3754–3764, 2012, doi: 10.1016/J.ACTBIO.2012.06.028.

[31] Y. Park, M. Sugimoto, A. Watrin, M. Chiquet, and E. B. Hunziker, "BMP-2 induces the expression of chondrocyte-specific genes in bovine synovium-derived progenitor cells cultured in three-dimensional alginate hydrogel," *Osteoarthritis Cartilage*, vol. 13, no. 6, pp. 527–536, Jun. 2005, doi: 10.1016/J.JOCA.2005.02.006.

[32] K. Ma, A. L. Titan, M. Stafford, C. H. Zheng, and M. E. Levenston, "Variations in chondrogenesis of human bone marrow-derived mesenchymal stem cells in fibrin/alginate blended hydrogels," *Acta Biomater*, vol. 8, no. 10, pp. 3754–3764, 2012, doi: 10.1016/J.ACTBIO.2012.06.028.

[33] C. Gerard *et al.*, "The effect of alginate, hyaluronate and hyaluronate derivatives biomaterials on synthesis of non-articular chondrocyte extracellular matrix," *J Mater Sci Mater Med*, vol. 16, no. 6, pp. 541–551, Jun. 2005, doi: 10.1007/s10856-005-0530-3.

[34] J. E. Song *et al.*, "Effects of purified alginate sponge on the regeneration of chondrocytes: In vitro and in vivo," *J Biomater Sci Polym Ed*, vol. 26, no. 3, pp. 181–195, Feb. 2015, doi: 10.1080/09205063.2014.987570.

[35] H. J. Häuselmann *et al.*, "Adult human chondrocytes cultured in alginate form a matrix similar to native human articular cartilage," *Am J Physiol*, vol. 271, no. 3 Pt 1, 1996, doi: 10.1152/AJPCELL.1996.271.3.C742.

[36] M. Szekalska, A. Puciłowska, E. Szymańska, P. Ciosek, and K. Winnicka, "Alginate: Current Use and Future Perspectives in Pharmaceutical and Biomedical Applications," *Int J Polym Sci*, vol. 2016, 2016, doi: 10.1155/2016/7697031.

[37] S. Sambu, X. Xu, H. Ye, and Z. F. Cui, "Predicting the survival rate of mouse embryonic stem cells cryopreserved in alginate beads," *Proc Inst Mech Eng H*, vol. 225, no. 11, pp. 1092–1107, Nov. 2011, doi: 10.1177/0954411911418568.

[38] E. S. Place, L. Rojo, E. Gentleman, J. P. Sardinha, and M. M. Stevens, "Strontium- and zinc-alginate hydrogels for bone tissue engineering," *Tissue Eng Part A*, vol. 17, no. 21–22, pp. 2713–2722, Nov. 2011, doi: 10.1089/TEN.TEA.2011.0059.

[39] A. Moshaverinia *et al.*, "Alginate hydrogel as a promising scaffold for dental-derived stem cells: an in vitro study," *SpringerA Moshaverinia, C Chen, K Akiyama, S Ansari, X Xu, WW Chee, SR Schricker, S ShiJournal of Materials Science: Materials in Medicine, 2012•Springer*, vol. 23, no. 12, pp. 3041–3051, Dec. 2012, doi: 10.1007/s10856-012-4759-3.

[40] Y. Liang *et al.*, “An in situ formed biodegradable hydrogel for reconstruction of the corneal endothelium,” *Colloids Surf B Biointerfaces*, vol. 82, no. 1, pp. 1–7, Jan. 2011, doi: 10.1016/J.COLSURFB.2010.07.043.

[41] B. Balakrishnan and A. Jayakrishnan, “Self-cross-linking biopolymers as injectable in situ forming biodegradable scaffolds,” *Biomaterials*, vol. 26, no. 18, pp. 3941–3951, Jun. 2005, doi: 10.1016/J.BIOMATERIALS.2004.10.005.

[42] M. Grellier *et al.*, “The effect of the co-immobilization of human osteoprogenitors and endothelial cells within alginate microspheres on mineralization in a bone defect,” *Biomaterials*, vol. 30, no. 19, pp. 3271–3278, Jul. 2009, doi: 10.1016/J.BIOMATERIALS.2009.02.033.

[43] W. S. Kim, D. J. Mooney, P. R. Arany, K. Lee, N. Huebsch, and J. Kim, “Adipose tissue engineering using injectable, oxidized alginate hydrogels,” *Tissue Eng Part A*, vol. 18, no. 7–8, pp. 737–743, Apr. 2012, doi: 10.1089/TEN.TEA.2011.0250.

[44] A. B. Bello, D. Kim, D. Kim, H. Park, and S. H. Lee, “Engineering and Functionalization of Gelatin Biomaterials: From Cell Culture to Medical Applications,” *Tissue Eng Part B Rev*, vol. 26, no. 2, pp. 164–180, Apr. 2020, doi: 10.1089/TEN.TEB.2019.0256.

[45] M. C. Echave, L. S. Burgo, J. L. Pedraz, and G. Orive, “Gelatin as Biomaterial for Tissue Engineering,” *Curr Pharm Des*, vol. 23, no. 24, May 2017, doi: 10.2174/1381612823666170511123101.

[46] D. Seliktar, “Designing cell-compatible hydrogels for biomedical applications,” *Science (1979)*, vol. 336, no. 6085, pp. 1124–1128, Jun. 2012, doi: 10.1126/SCIENCE.1214804.

[47] M. C. Echave *et al.*, “Enzymatic crosslinked gelatin 3D scaffolds for bone tissue engineering,” *Int J Pharm*, vol. 562, pp. 151–161, May 2019, doi: 10.1016/J.IJPHARM.2019.02.043.

[48] Y. Liu *et al.*, “Tunable physical and mechanical properties of gelatin hydrogel after transglutaminase crosslinking on two gelatin types,” *Int J Biol Macromol*, vol. 162, pp. 405–413, Nov. 2020, doi: 10.1016/J.IJBIOMAC.2020.06.185.

[49] C. Guo, J. Wu, Y. Zeng, and H. Li, “Construction of 3D bioprinting of HAP/collagen scaffold in gelation bath for bone tissue engineering,” *Regen Biomater*, vol. 10, 2023, doi: 10.1093/RB/RBAD067.

[50] H. R. Lin and Y. J. Yen, “Porous alginate/hydroxyapatite composite scaffolds for bone tissue engineering: Preparation, characterization, and in vitro studies,”

J Biomed Mater Res B Appl Biomater, vol. 71, no. 1, pp. 52–65, Oct. 2004, doi: 10.1002/jbm.b.30065.

[51] M. O. Christen and F. Vercesi, “Polycaprolactone: How a well-known and futuristic polymer has become an innovative collagen-stimulator in esthetics,” *Clin Cosmet Investig Dermatol*, vol. 13, pp. 31–48, 2020, doi: 10.2147/CCID.S229054.

[52] R. Dwivedi *et al.*, “Polycaprolactone as biomaterial for bone scaffolds: Review of literature,” *J Oral Biol Craniofac Res*, vol. 10, no. 1, p. 381, Jan. 2020, doi: 10.1016/J.JOBCR.2019.10.003.

[53] C. Erisken, X. Zhang, K. L. Moffat, W. N. Levine, and H. H. Lu, “Scaffold fiber diameter regulates human tendon fibroblast growth and differentiation,” *Tissue Eng Part A*, vol. 19, no. 3–4, pp. 519–528, Feb. 2013, doi: 10.1089/ten.tea.2012.0072.

[54] S. Kadyr *et al.*, “Braided biomimetic PCL grafts for anterior cruciate ligament repair and regeneration,” *Biomedical Materials*, vol. 19, no. 2, p. 025034, Mar. 2024, doi: 10.1088/1748-605X/ad2555.

[55] V. Kokol, Y. B. Pottathara, M. Mihelčič, and L. S. Perše, “Rheological properties of gelatine hydrogels affected by flow- and horizontally-induced cooling rates during 3D cryo-printing,” *Colloids Surf A Physicochem Eng Asp*, vol. 616, May 2021, doi: 10.1016/j.colsurfa.2021.126356.

[56] C. Erisken, D. M. Kalyon, and H. Wang, “Functionally graded electrospun polycaprolactone and β-tricalcium phosphate nanocomposites for tissue engineering applications,” *Biomaterials*, vol. 29, no. 30, pp. 4065–4073, Oct. 2008, doi: 10.1016/j.biomaterials.2008.06.022.

[57] C. Erisken, D. M. Kalyon, H. Wang, C. Ornek-Ballanco, and J. Xu, “Osteochondral tissue formation through adipose-derived stromal cell differentiation on biomimetic polycaprolactone nanofibrous scaffolds with graded insulin and Beta-glycerophosphate concentrations.,” *Tissue Eng Part A*, vol. 17, no. 9–10, pp. 1239–52, May 2011, doi: 10.1089/ten.TEA.2009.0693.

[58] E. Kon *et al.*, “Novel nanostructured scaffold for osteochondral regeneration: pilot study in horses,” *J Tissue Eng Regen Med*, vol. 4, no. 4, Jan. 2010, doi: 10.1002/term.243.

[59] X. Barceló, K. F. Eichholz, O. Garcia, and D. J. Kelly, “Tuning the Degradation Rate of Alginate-Based Bioinks for Bioprinting Functional Cartilage Tissue.,” *Biomedicines*, vol. 10, no. 7, Jul. 2022, doi: 10.3390/biomedicines10071621.

[60] C. Erisken, D. M. Kalyon, and H. Wang, “Functionally graded electrospun polycaprolactone and beta-tricalcium phosphate nanocomposites for tissue engineering applications,” *Biomaterials*, vol. 29, no. 30, pp. 4065–4073, 2008, doi: 10.1016/j.biomaterials.2008.06.022.